ARTICLE

On-Surface Debromination of C_6Br_6: C_6 Ring versus C_6 Chain

Wenze Gao,[#] Faming Kang,[#] Xia Qiu,[#] Zewei Yi, Lina Shang, Mengxi Liu,* Xiaohui Qiu, Yi Luo,* and Wei Xu*

Read Online

ACCESS | Metrics & More | Article Recommendations | Supporting Information

ABSTRACT: Carbon allotropes comprising sp-hybridized carbon atoms have been investigated for decades for their molecular structure. One of the unsolved mysteries is whether they should take a linear or cyclic configuration in condensed phases due to the lack of atomistic characterizations. Herein, we designed a molecule with a C_6 skeleton as a model system to address this issue, which was achieved by eliminating Br atoms from hexabromobenzene (C_6Br_6) molecule on the Ag(111) substrate via thermal treatment. It is found that the C_6 ring intermediate resulting from complete debromination is energetically unstable at room temperature based on theoretical calculations. It subsequently transforms into the C_6 polyynic chain via a ring-opening process and ultimately polymerizes into the organometallic polyyne, whose triyne structural unit is revealed by bond-resolved noncontact atomic force microscopy. Theoretical calculations demonstrated an energetically favorable pathway in which the ring-opening process occurs after complete debromination of C_6Br_6. Our study provides a platform for the synthesis of elusive carbon-rich materials.

KEYWORDS: C_6 allotropes, ring opening, organometallic polyyne, scanning tunneling microscopy, atomic force microscopy

Carbon allotropes have gained a significant interest since the successive discoveries of fullerenes,[1] carbon nanotubes,[2] and graphene,[3] all of which are sp²-hybridized carbon allotropes and exhibit extraordinary properties. The sp-hybridized carbon allotropes such as rings and chains of two-coordinate carbon atoms, known as cyclocarbons and carbyne, have also excited chemists for decades.[4−7] The C_6 allotrope, in particular, has attracted much attention for its possibility of being the smallest carbon ring theoretically since such a structure can be expected to have a stabilization resulting from its cyclic conjugated system with $(4n + 2)\pi$ electrons according to Hückel's rule.[8] Whether the ground state of C_6 is linear or cyclic has always been a fundamental and controversial question (Figure 1a).[4,9−11]

The molecular structure of C_6 has been a topic of debate since Pitzer and Clementi discussed the stability of C_6 in 1959.[12] Most results depend on the level of theory and still have no clear conclusion whether the ground state of C_6 is a carbon ring or a carbon chain in the gas phase. Most Hartree−Fock and Møller−Plesset perturbation theory calculations[8,10] and coupled-cluster methods[13,14] predict that the carbon ring is the ground state of C_6. In contrast, density functional tight-binding theory,[15] semiempirical calculations,[12] and multireference configuration interaction methods[16] predict that the lowest energy molecular structure of C_6 is the carbon chain. There is also experimental evidence for the existence of
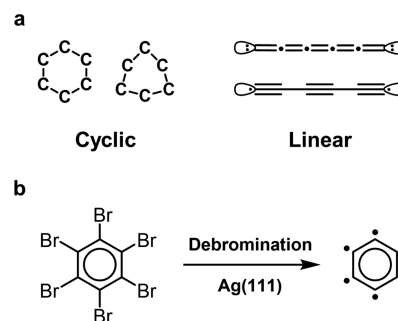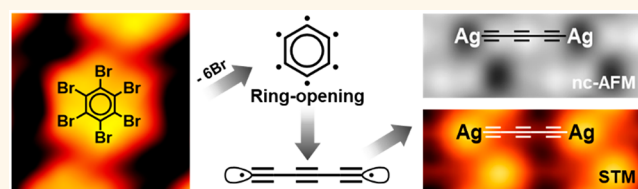

Figure 1. C_6 allotropes and a potential route to C_6 from C_6Br_6 molecular precursor. (a) Possible structures of C_6 allotropes proposed by refs 14 and 16. (b) Schematic illustration of our scheme of on-surface debromination of C_6Br_6.
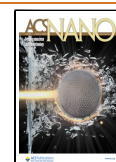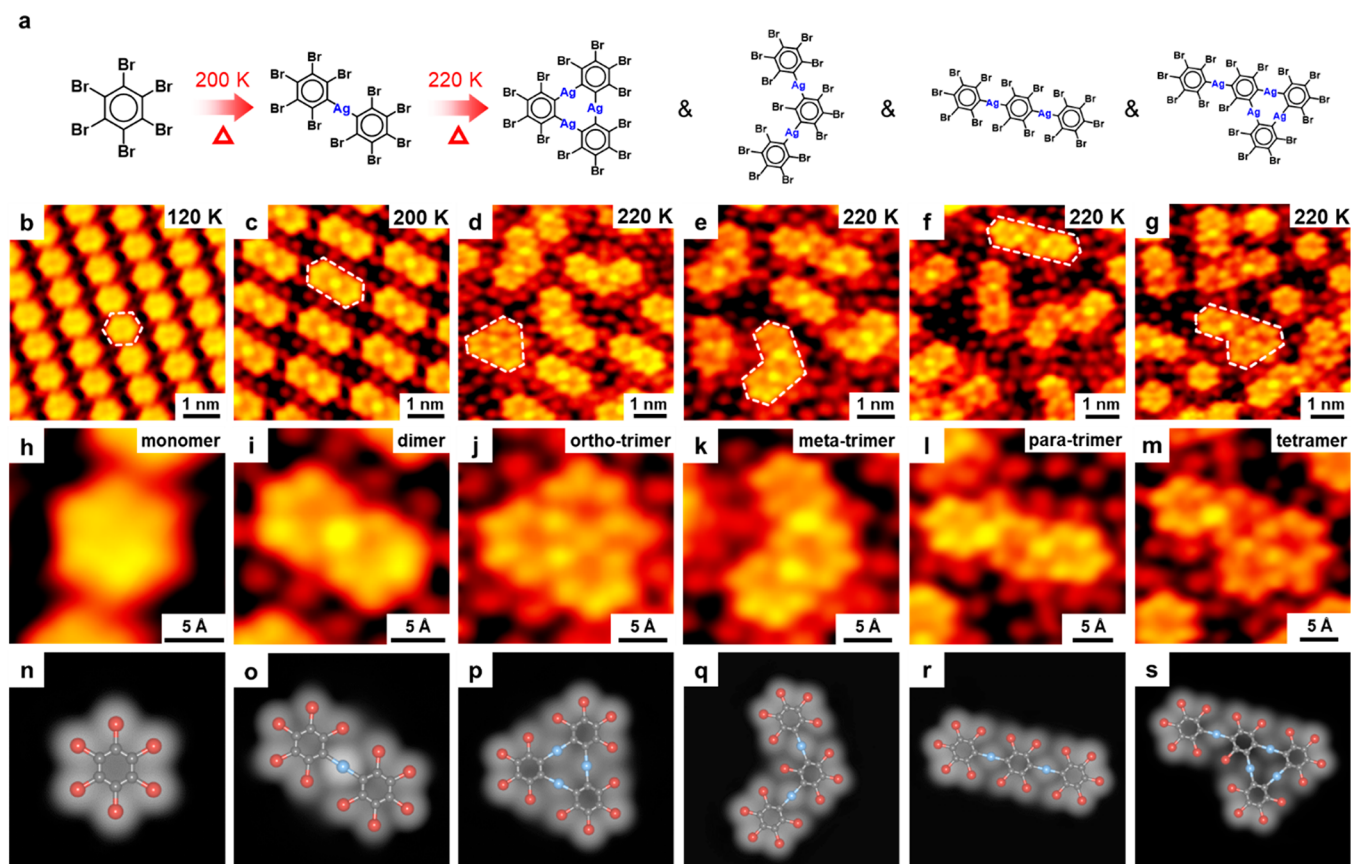
Figure 2. Sequential annealing induced organometallic coupling reactions of C_6Br_6 on Ag(111). (a) Reaction scheme from C_6Br_6 to organometallic oligomers. (b) Large-scale STM image of individual C_6Br_6 molecules adsorbed on the surface at 120 K. The individual molecule is highlighted by a white contour. (c–g) Large-scale STM images of debrominative organometallic coupling products obtained by sequential annealing processes. The various reaction products are highlighted by white contours. (h–m) Close-up STM images of C_6Br_6 monomer and various organometallic products. (n–s) Corresponding simulated STM images with top-view DFT models overlaid. Gray, red, and blue balls represent C, Br, and Ag atoms, respectively. $V_t = -883$ mV; $I_t = 0.94$ nA.

both cyclic and linear C_6 in the gas phase,[17,18] but these C_6 allotropes have not been structurally characterized at the atomic level or studied on the surface.

On-surface synthesis provides a convenient alternative approach for atomically precise fabrication of nanostructures,[19,20] which requires further elaborate characterization. The developments of scanning tunneling microscopy (STM) and noncontact atomic force microscopy (nc-AFM) allow us to characterize the structure of molecules with atomic resolution.[6] In this work, we investigate the C_6Br_6 molecule on the Ag(111) surface. In comparison with the inert Au(111)[21] and HOPG/MoS_2[22] surface, the relatively high chemical activity of the Ag(111) surface allows the C_6Br_6 molecule to be completely debrominated at room temperature (RT), thus providing an opportunity to obtain a C_6 ring on the surface (Figure 1b). As such, the molecular structure of C_6 could be explored with respect to the controversial question mentioned above. Here, by the combination of high-resolution STM, nc-AFM, and density functional theory (DFT) calculations, we demonstrated that complete debromination of the C_6Br_6 molecule could occur at RT on the Ag(111) surface, and the C_6 ring intermediate is theoretically speculated to be unstable, which subsequently transforms into the C_6 polyynic chain via a ring-opening process and finally polymerizes into the organometallic polyynes. The organometallic polyynes were experimentally observed by nc-AFM,

which allows identifying the alternating single and triple bonds within C_6 moieties. Theoretical calculations demonstrated that the ring-opening process occurs after complete debromination of C_6Br_6. This study further expands the database of on-surface debromination and ring-opening reactions and provides us with an alternative strategy for the synthesis of elusive carbon-rich materials, which would inspire further characterizations toward understanding the nature of low-dimensional nanostructures containing sp-hybridized C_6 at the atomic scale.

RESULTS AND DISCUSSION

The C_6Br_6 molecule was deposited on Ag(111) at 120 K to obtain an individual molecule, and then we gradually increased the substrate temperature to eliminate Br atoms from C_6Br_6 molecules (Figure 2a). After deposition, a self-assembled molecular island was observed, as shown in Figure 2b, in which the individual C_6Br_6 molecule was highlighted by the hexagonal contour. The C_6Br_6 monomer appeared as a hexagonal motif with six bright protrusions at the corners, as shown in the close-up STM image (Figure 2h). The six bright protrusions were assigned to Br atoms.[21] Upon annealing the sample to ~200 K, a kind of dimer structure highlighted by the white contour was observed, as shown in Figure 2c. The close-up STM image in Figure 2i shows that the dimer structure is the product of debrominative organometallic coupling of C_6Br_6, in which the bright protrusion in the middle of the

dimer is assigned to the Ag atom. Similar structures have been widely reported and proven to be organometallic intermediates in the Ullmann coupling process.[23−25] Further annealing to ~220 K resulted in various trimeric and tetrameric organometallic structures formed by further debromination of C_6Br_6 molecules (Figure 2d−g). For example, we observed three different sites of debromination with respect to the individual molecule, resulting in *ortho-*, *meta-*, and *para-*trimers, respectively, as shown in the close-up STM images in Figure 2j−l. Meanwhile, the tetramer in which a C_6Br_6 molecule has already detached three Br atoms was also observed, as shown in Figure 2g,m. The assignment of the C_6Br_6 molecule and various organometallic intermediates was further supported by STM simulations with DFT-calculated models overlaid (Figure 2n−s). Nearly 60% of the oligomers were desorbed from the substrate after annealing to ~270 K (Supporting Information, Figure S1e). Finally, the sample was annealed to RT (300 K), resulting in the formation of disordered organometallic coupling products of C_6Br_6 (Supporting Information, Figure S 1f). As shown above, only the formation of various organometallic intermediates is observed during sequential annealing processes.

To avoid debrominative organometallic coupling induced by sequential annealing and to obtain the fully debrominated product of C_6Br_6, we tried to directly deposit C_6Br_6 on the Ag(111) kept at increased temperatures of 220, 240, 270, and 300 K. Depositing C_6Br_6 onto the Ag(111) surface held at 220 K and below shows the same results (Figure 3a) as sequential
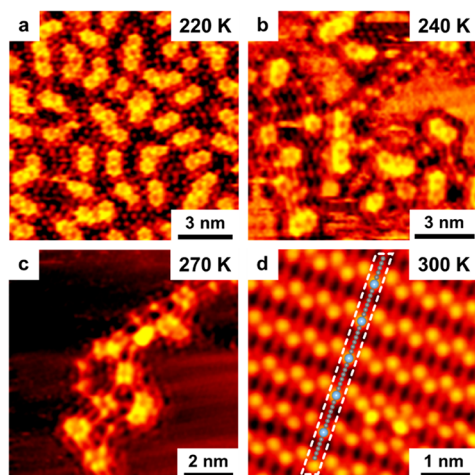

Figure 3. Reaction products of C_6Br_6 on Ag(111) at different substrate temperatures. (a−d) STM images of reaction products formed by deposition of C_6Br_6 onto the substrate at (a) 220 K, (b) 240 K, (c) 270 K, and (d) 300 K. The individual organometallic polyyne is highlighted by the white contour with the structural model overlaid. Molecular evaporation temperature: 355 K; deposition time: 20 s. $V_t = −743$ mV; $I_t = 1.28$ nA.

annealing from 120 to 220 K shown previously. However, different debrominative organometallic coupling products began to deposit C_6Br_6 on the Ag(111) held at 240−270 K, that is, 1-D chain structures mixed with previously observed organometallic oligomers, as shown in Figure 3b,c. Surprisingly, with the substrate temperature increased to 300 K followed by deposition of C_6Br_6, only 1-D chain structures can be observed, as shown in Figure 3d. Interestingly, such chain structures resemble the previously reported Cu/Au-incorpo-

rated organometallic carbon chains.[26,27] The experimental periodicity of the chain structure is 11 ± 0.3 Å (Supporting Information, Figure S2), in comparison with C_2−Cu and C_4−Au organometallic carbon chains,[26,27] so we then naturally attribute this 1-D chain structure to the C_6−Ag organometallic carbon chain.

To further verify the formation of the C_6−Ag organometallic carbon chain and clarify its atomic-scale structure, we used high-resolution STM and nc-AFM imaging in conjunction with extensive DFT calculations. Figure 4a shows close-packed C_6−Ag organometallic carbon chains (a large-scale STM image is shown in Supporting Information, Figure S3). The close-up nc-AFM image (Figure 4b) and STM image (Figure 4c) clearly resolved the chemical structure of the organometallic carbon chains, in which the Ag atoms are imaged as protrusions and depressions in STM and nc-AFM images, respectively, agreeing well with the early studies.[26,27] The C_6 moiety in the nc-AFM image shows three discrete characteristic protrusions which are assigned to the three adjacent C−C triple bonds, revealing the nature of the polyyynic segment.[28,29] This undoubtedly confirms the formation of the C_6−Ag organometallic polyyne on the Ag(111) surface. Experimental observations were further supported by DFT calculations (see Figures S4 and S5 in Supporting Information for a comparison between different adsorption configurations of the organometallic polyyne assembly structures), with the simulated STM image agreeing well with the experiments (Figure 4d). Moreover, the scanning tunneling spectroscopy (STS) showed an experimental band gap of ~1.3 eV on the Ag(111) surface, indicating the semiconducting characteristic of the organometallic polyyne (Supporting Information, Figure S6).

Thus, from the results discussed above, the whole scenario can be speculated below (Figure 4e): complete debromination of C_6Br_6 should occur on the Ag(111) surface at RT, which could then result in the formation of a C_6 ring intermediate that was not stable and broken into the C_6 chain via a ring-opening process and finally polymerized into the observed organometallic polyyne. According to previous studies, the surface-stabilized carbene (=C:) could directly couple into the cumulene structure without bonding to a metal adatom,[30,31] whereas the dehalogenated terminal alkynyl group (≡C·) would form organometallic structures on metal surfaces.[32,33] Therefore, the formation of C_6−Ag organometallic polyyne implied the individual C_6 chain should be polyyynic instead of cumulenic.

To further verify our hypothesis of the complete debromination of C_6Br_6 and ring opening of C_6, we calculated the reaction pathways from the C_6Br_6 molecular precursor to the C_6 ring through successive C−Br bond activations (Figure 5a) and subsequent ring-opening processes on Ag(111) (Figure 5b,c) with DFT-based transition state theory. The energetically most favorable reaction pathway for the sequential C−Br bond activations of C_6Br_6 on Ag(111) is shown in Figure 5a. Alternative less favorable reaction pathways are illustrated in the Supporting Information, Figures S7−S11. The complete debromination requires six sequential steps of C−Br bond cleavage that converted C_6Br_6 into the C_6 ring residue, with the highest energy barrier of 0.76 eV. The debromination process is exothermic with a reaction energy of −1.63 eV. Notably, DFT calculations revealed that two adjacent phenyl radicals in **Int2** were chemisorbed on the surface after the *ortho-*Br atom of **Int1** is detached, resulting in the C_6Br_4 intermediate being bonded upright to the Ag(111)
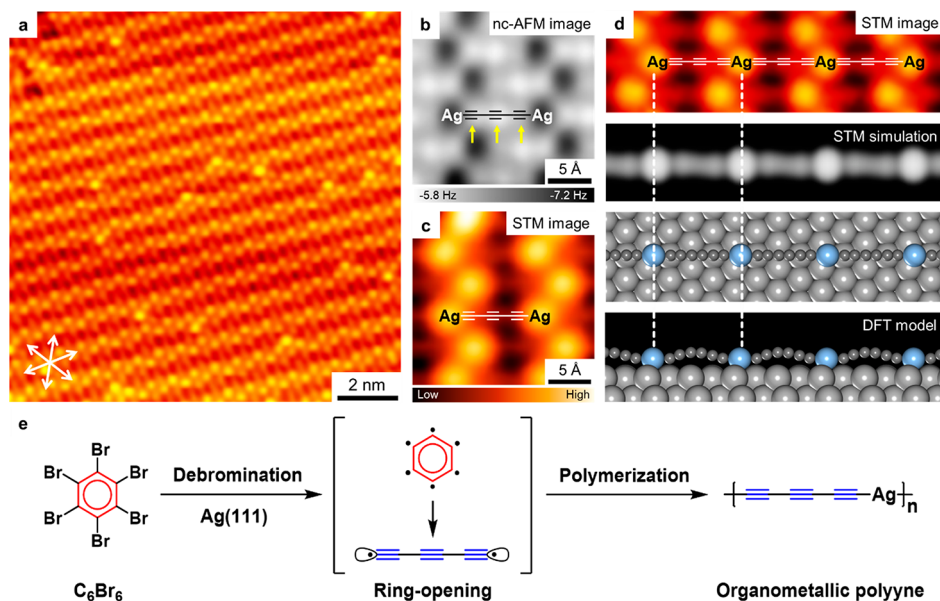
Figure 4. Structural properties of the organometallic polyyne and reaction scheme of C_6Br_6 on Ag(111). (a) Large-scale STM image showing the formation of organometallic polyynes on the Ag(111) surface by depositing C_6Br_6 molecules on the sample held at 300 K. (b) Constant-height nc-AFM image and (c) corresponding STM image of organometallic polyynes, in which the triyne moieties within these chains are identified from the nc-AFM images, as indicated by yellow arrows. (d) From top to bottom: an STM image, a simulated STM image, and top- and side-view DFT models of a single organometallic polyyne on Ag(111). (e) Schematic illustration showing the formation of organometallic polyyne from C_6Br_6. Scanning conditions: (a,d) $V_t = -625$ mV; $I_t = 1.58$ nA; (b) $V_t = 0$ mV; the tip height is set close to the sample by 280 pm with respect to the STM set point: $V_t = -1$ V, $I_t = 0.1$ nA; (c) $V_t = -1000$ mV; $I_t = 0.1$ nA.

substrate. Importantly, the following intermediates were kept upright until the whole debromination process proceeded.

Next, we investigated the ring-opening process. Starting from the FS (with the C_6 ring being upright to the Ag(111) surface) shown in Figure 5a, it is seen that the ring-opening reaction barrier is 0.73 eV, as shown in Figure 5b. The barriers for the ring-opening process are increased to 0.99 eV with the C_6 ring being flat to the Ag(111) surface (Figure 5c) and 2.60 eV in the gas phase (Supporting Information, Figure S12). Comparison of Figure 5b,c indicates that the reduced reaction energy barrier of 0.26 eV results from the adsorption configuration of the C_6 ring. The upright adsorption configuration of the C_6 ring reduces the distance between the target C−C bond (ring-opening site) and the surface Ag atoms, which creates a surface catalytic effect stronger than that of the flat one.

Further DFT calculations on the competitive reaction pathways between ring-opening and debromination processes of C_6Br_3, C_6Br_2, and C_6Br intermediates were also performed (Supporting Information, Figure S13). It is seen that the energy barriers of debromination are always lower than that of the corresponding ring opening, showing that, although there is no direct experimental evidence on the formation of cyclic C_6 structure, our hypothesis of the ring-opening process occurring after complete debromination of C_6Br_6 is theoretically reasonable. The ring-opening process is highly exothermic with a reaction energy of −2.27 eV (Figure 5b), indicating the energetic favorability of the ring-opening process of the C_6 ring on the Ag(111) surface.

CONCLUSIONS

We have demonstrated that the C_6Br_6 molecule could undergo complete debromination on the Ag(111) surface at RT, resulting in the C_6 ring intermediate based on the DTF

calculations. However, the C_6 ring breaks into a C_6 chain on the surface at RT from an energetic point of view, which subsequently leads to the formation of C_6−Ag organometallic polyyne, and the C_6 moiety is experimentally confirmed to be triyne. Our results present complementary insights into the debromination, ring opening, and organometallic coupling processes of C_6Br_6 on the surface and provide an alternative strategy for the synthesis of other sp-hybridized 1-D carbon nanostructures that are rarely synthesized via conventional solution chemistry. The revealed semiconductivity of the organometallic polyynes also makes it a candidate for molecular electronic devices.

METHODS

STM/nc-AFM Measurements. A variable-temperature "Aarhus-type" STM[34,35] was used for performing the STM experiments in situ, including sample preparation, molecular evaporation, and characterization under ultra-high-vacuum conditions (base pressure below 3×10^{-10} mbar). The STM images in Figure S1 were recorded at the varied temperature along with the sample preparation condition. Other STM images were recorded at 100 K. A low-temperature Scienta Omicron STM/AFM was used for performing the nc-AFM experiments under ultra-high-vacuum conditions (base pressure below 1×10^{-10} mbar). The Ag(111) single crystal was cleaned by cycles of 1.5 keV argon ion sputtering followed by annealing at 800 K for 15 min. The C_6Br_6 molecules were deposited into the ultra-high-vacuum chamber through a molecular evaporator. The STM images were recorded in constant-current mode, and the nc-AFM images were recorded in constant-height mode with a Br-functionalized tip based on a qPlus sensor design[36] at liquid helium temperature (oscillation amplitude $A = 170$ pm, quality factor $Q = 8 \times 10^4$, resonance frequency $f_0 = 42.15$ kHz).

Theoretical Calculations. The structural optimizations of organometallic polyynes on the Ag(111) were performed by using the Vienna ab initio simulation package (VASP) code[37,38] in the framework of DFT calculations. The projector-augmented wave method[39,40] was used to describe the interaction between ions and
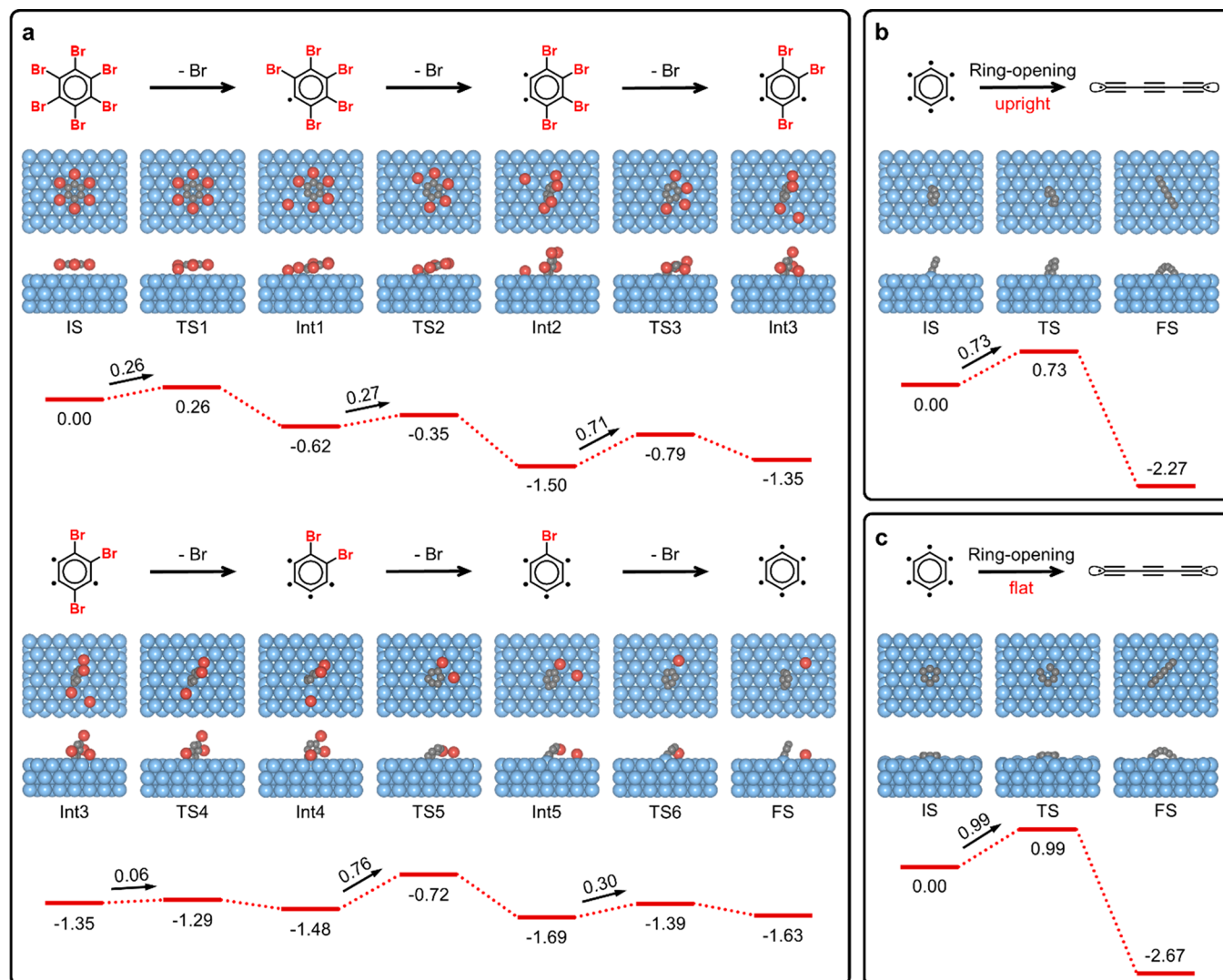
Figure 5. Reaction pathways for the debromination of C_6Br_6 and ring opening of C_6 processes. (a) DFT-calculated energetically the most favorable reaction pathway for the sequential C–Br bond activations of C_6Br_6 on Ag(111). (b,c) DFT-calculated reaction pathways of the ring-opening process of the C_6 ring which is (b) in an upright and (c) in a flat conformation with respect to the Ag(111) surface. The structural models are given for the initial (IS), transition (TS), and final states (FS). Energies are given in units of eV.

electrons. The kinetic energy cutoff was set to 400 eV. The van der Waals density functional (vdW-DF)[41] was used to describe the exchange-correlation effects using the version by Hamada denoted as rev-vdWDF2.[42] For the debromination and ring-opening calculations, we used a $p(6 \times 6)$ surface unit cell of Ag(111) with a $2 \times 2 \times 1$ gamma centered Monkhorst–Pack k-point grid. Transition states were found by the climbing image nudged elastic band (CI-NEB)[43] and dimer methods,[44] and all local minima and saddle points were optimized until the forces on all unconstrained atoms were ≤0.03 eV/ Å. The Tersoff–Hamann method[45] was used to obtain the simulated STM image.

ASSOCIATED CONTENT

Ⓢ Supporting Information

The Supporting Information is available free of charge at https://pubs.acs.org/doi/10.1021/acsnano.2c00945.

STM images showing the sequential annealing process of C_6Br_6 on Ag(111); line-scan profile and larger-scale STM image of organometallic polyynes; dI/dV spectra of the organometallic polyyne taken on the Ag(111) surface; additional DFT calculations on adsorption

configurations, debromination, and ring-opening processes of C_6Br_6 (PDF)

AUTHOR INFORMATION

Corresponding Authors

Wei Xu − *Interdisciplinary Materials Research Center, College of Materials Science and Engineering, Tongji University, Shanghai 201804, People's Republic of China;* ⓘ orcid.org/ 0000-0003-0216-794X; Email: xuwei@tongji.edu.cn

Yi Luo − *Hefei National Laboratory for Physical Sciences at the Microscale & Department of Chemical Physics, iChEM, University of Science and Technology of China, Hefei, Anhui 230026, People's Republic of China;* Email: yiluo@ ustc.edu.cn

Mengxi Liu − *CAS Key Laboratory of Standardization and Measurement for Nanotechnology, CAS Center for Excellence in Nanoscience, National Center for Nanoscience and Technology, Beijing 100190, People's Republic of China;* ⓘ orcid.org/0000-0001-7009-5269; Email: liumx@ nanoctr.cn

Authors

Wenze Gao − *Interdisciplinary Materials Research Center, College of Materials Science and Engineering, Tongji University, Shanghai 201804, People's Republic of China*

Faming Kang − *Interdisciplinary Materials Research Center, College of Materials Science and Engineering, Tongji University, Shanghai 201804, People's Republic of China*

Xia Qiu − *CAS Key Laboratory of Standardization and Measurement for Nanotechnology, CAS Center for Excellence in Nanoscience, National Center for Nanoscience and Technology, Beijing 100190, People's Republic of China; University of Chinese Academy of Sciences, Beijing 100049, People's Republic of China; Academy for Advanced Interdisciplinary Studies, Peking University, Beijing 100871, People's Republic of China*

Zewei Yi − *Interdisciplinary Materials Research Center, College of Materials Science and Engineering, Tongji University, Shanghai 201804, People's Republic of China*

Lina Shang − *Interdisciplinary Materials Research Center, College of Materials Science and Engineering, Tongji University, Shanghai 201804, People's Republic of China*

Xiaohui Qiu − *CAS Key Laboratory of Standardization and Measurement for Nanotechnology, CAS Center for Excellence in Nanoscience, National Center for Nanoscience and Technology, Beijing 100190, People's Republic of China; University of Chinese Academy of Sciences, Beijing 100049, People's Republic of China*

Complete contact information is available at:
https://pubs.acs.org/10.1021/acsnano.2c00945

Author Contributions

Notes

ACKNOWLEDGMENTS

REFERENCES

(1) Kroto, H. W.; Heath, J. R.; O'Brien, S. C.; Curl, R. F.; Smalley, R. E. C_{60}: Buckminsterfullerene. *Nature* **1985**, *318*, 162−163.

(2) Iijima, S.; Ichihashi, T. Single-Shell Carbon Nanotubes of 1-nm Diameter. *Nature* **1993**, *363*, 603−605.

(3) Novoselov, K. S.; Geim, A. K.; Morozov, S. V.; Jiang, D.; Zhang, Y.; Dubonos, S. V.; Grigorieva, I. V.; Firsov, A. A. Electric Field Effect in Atomically Thin Carbon Films. *Science* **2004**, *306*, 666−669.

(4) Hoffmann, R. Extended Hückel Theory—V. *Tetrahedron* **1966**, *22*, 521−538.

(5) Diederich, F.; Rubin, Y.; Knobler, C. B.; Whetten, R. L.; Schriver, K. E.; Houk, K. N.; Li, Y. All-Carbon Molecules: Evidence for the Generation of Cyclo[18]carbon from a Stable Organic Precursor. *Science* **1989**, *245*, 1088−1090.

(6) Kaiser, K.; Scriven, L. M.; Schulz, F.; Gawel, P.; Gross, L.; Anderson, H. L. An *Sp*-Hybridized Molecular Carbon Allotrope, Cyclo[18]carbon. *Science* **2019**, *365*, 1299−1301.

(7) Shi, L.; Rohringer, P.; Suenaga, K.; Niimi, Y.; Kotakoski, J.; Meyer, J. C.; Peterlik, H.; Wanko, M.; Cahangirov, S.; Rubio, A.; Lapin, Z. J.; Novotny, L.; Ayala, P.; Pichler, T. Confined Linear Carbon Chains as a Route to Bulk Carbyne. *Nat. Mater.* **2016**, *15*, 634−639.

(8) Raghavachari, K.; Whiteside, R. A.; Pople, J. A. Structures of Small Carbon Clusters: Cyclic Ground State of C_6. *J. Chem. Phys.* **1986**, *85*, 6623−6628.

(9) Belau, L.; Wheeler, S. E.; Ticknor, B. W.; Ahmed, M.; Leone, S. R.; Allen, W. D.; Schaefer, H. F.; Duncan, M. A. Ionization Thresholds of Small Carbon Clusters: Tunable VUV Experiments and Theory. *J. Am. Chem. Soc.* **2007**, *129*, 10229−10243.

(10) Raghavachari, K.; Binkley, J. S. Structure, Stability, and Fragmentation of Small Carbon Clusters. *J. Chem. Phys.* **1987**, *87*, 2191−2197.

(11) von Helden, G.; Hsu, M.-T.; Kemper, P. R.; Bowers, M. T. Structures of Carbon Cluster Ions from 3 to 60 Atoms: Linears to Rings to Fullerenes. *J. Chem. Phys.* **1991**, *95*, 3835−3837.

(12) Pitzer, K. S.; Clementi, E. Large Molecules in Carbon Vapor. *J. Am. Chem. Soc.* **1959**, *81*, 4477−4485.

(13) Martin, J. M. L.; Taylor, P. R. Accurate *Ab Initio* Total Atomization Energies of the C_n Clusters (n = 2−10). *J. Chem. Phys.* **1995**, *102*, 8270−8273.

(14) Hutter, J.; Lüthi, H. P. The Molecular Structure of C_6: A Theoretical Investigation. *J. Chem. Phys.* **1994**, *101*, 2213−2216.

(15) Yen, T. W.; Lai, S. K. Use of Density Functional Theory Method to Calculate Structures of Neutral Carbon Clusters C_n ($3 \leq n \leq 24$) and Study Their Variability of Structural Forms. *J. Chem. Phys.* **2015**, *142*, 084313.

(16) Parasuk, V.; Almlöf, J. The Electronic and Molecular Structure of C_6: Complete Active Space Self-Consistent-Field and Multi-reference Configuration Interaction. *J. Chem. Phys.* **1989**, *91*, 1137−1141.

(17) Wang, S. L.; Rittby, C. M. L.; Graham, W. R. M. Detection of Cyclic Carbon Clusters. I. Isotopic Study of the $v_4(e')$ Mode of Cyclic C_6 in Solid Ar. *J. Chem. Phys.* **1997**, *107*, 6032−6037.

(18) Van Zee, R. J.; Ferrante, R. F.; Zeringue, K. J.; Weltner, W.; Ewing, D. W. Electron Spin Resonance of the C_6, C_8, and C_{10} Molecules. *J. Chem. Phys.* **1988**, *88*, 3465−3474.

(19) Grill, L.; Dyer, M.; Lafferentz, L.; Persson, M.; Peters, M. V.; Hecht, S. Nano-Architectures by Covalent Assembly of Molecular Building Blocks. *Nat. Nanotechnol.* **2007**, *2*, 687−691.

(20) Clair, S.; de Oteyza, D. G. Controlling a Chemical Coupling Reaction on a Surface: Tools and Strategies for On-Surface Synthesis. *Chem. Rev.* **2019**, *119*, 4717−4776.

(21) Huang, H.; Tan, Z.; He, Y.; Liu, J.; Sun, J.; Zhao, K.; Zhou, Z.; Tian, G.; Wong, S. L.; Wee, A. T. S. Competition between Hexagonal and Tetragonal Hexabromobenzene Packing on Au(111). *ACS Nano* **2016**, *10*, 3198−3205.

(22) Strohmaier, R.; Ludwig, C.; Petersen, J.; Gompf, B.; Eisenmenger. STM Investigations of C_6Br_6 on HOPG and MoS_2. *Surf. Sci.* **1994**, *318*, L1181−L1185.

(23) Fan, Q.; Wang, C.; Han, Y.; Zhu, J.; Hieringer, W.; Kuttner, J.; Hilt, G.; Gottfried, J. M. Surface-Assisted Organic Synthesis of Hyperbenzene Nanotroughs. *Angew. Chem., Int. Ed.* **2013**, *52*, 4668−4672.

(24) Wang, W.; Shi, X.; Wang, S.; Van Hove, M. A.; Lin, N. Single-Molecule Resolution of an Organometallic Intermediate in a Surface-Supported Ullmann Coupling Reaction. *J. Am. Chem. Soc.* **2011**, *133*, 13264−13267.

(25) Walch, H.; Gutzler, R.; Sirtl, T.; Eder, G.; Lackinger, M. Material- and Orientation-Dependent Reactivity for Heterogeneously Catalyzed Carbon-Bromine Bond Homolysis. *J. Phys. Chem. C* **2010**, *114*, 12604−12609.

(26) Yu, X.; Li, X.; Lin, H.; Liu, M.; Cai, L.; Qiu, X.; Yang, D.; Fan, X.; Qiu, X.; Xu, W. Bond-Scission-Induced Structural Transformation from Cumulene to Diyne Moiety and Formation of Semiconducting Organometallic Polyyne. *J. Am. Chem. Soc.* **2020**, *142*, 8085−8089.

(27) Sun, Q.; Cai, L.; Wang, S.; Widmer, R.; Ju, H.; Zhu, J.; Li, L.; He, Y.; Ruffieux, P.; Fasel, R.; Xu, W. Bottom-Up Synthesis of Metalated Carbyne. *J. Am. Chem. Soc.* **2016**, *138*, 1106−1109.

(28) de Oteyza, D. G.; Gorman, P.; Chen, Y. C.; Wickenburg, S.; Riss, A.; Mowbray, D. J.; Etkin, G.; Pedramrazi, Z.; Tsai, H. Z.; Rubio, A.; Crommie, M. F.; Fischer, F. R. Direct Imaging of Covalent Bond Structure in Single-Molecule Chemical Reactions. *Science* **2013**, *340*, 1434−1437.

(29) Pavliček, N.; Gawel, P.; Kohn, D. R.; Majzik, Z.; Xiong, Y.; Meyer, G.; Anderson, H. L.; Gross, L. Polyyne Formation *via* Skeletal Rearrangement Induced by Atomic Manipulation. *Nat. Chem.* **2018**, *10*, 853−858.

(30) Sun, Q.; Tran, B. V.; Cai, L.; Ma, H.; Yu, X.; Yuan, C.; Stöhr, M.; Xu, W. On-Surface Formation of Cumulene by Dehalogenative Homocoupling of Alkenyl *gem*-Dibromides. *Angew. Chem., Int. Ed.* **2017**, *56*, 12165−12169.

(31) Cai, L.; Kang, F.; Sun, Q.; Gao, W.; Yu, X.; Ma, H.; Yuan, C.; Xu, W. The Stereoselective Formation of trans-Cumulene through Dehalogenative Homocoupling of Alkenyl *gem*-Dibromides on Cu(110). *ChemCatChem.* **2019**, *11*, 5417−5420.

(32) Shu, C.; He, Y.; Zhang, R.; Chen, J.; Wang, A.; Liu, P. Atomic-Scale Visualization of Stepwise Growth Mechanism of Metal-Alkynyl Networks on Surfaces. *J. Am. Chem. Soc.* **2020**, *142*, 16579−16586.

(33) Sun, Q.; Cai, L.; Ma, H.; Yuan, C.; Xu, W. Dehalogenative Homocoupling of Terminal Alkynyl Bromides on Au(111): Incorporation of Acetylenic Scaffolding into Surface Nanostructures. *ACS Nano* **2016**, *10*, 7023−7030.

(34) Laegsgaard, E.; Österlund, L.; Thostrup, P.; Rasmussen, P. B.; Stensgaard, I.; Besenbacher, F. A High-Pressure Scanning Tunneling Microscope. *Rev. Sci. Instrum.* **2001**, *72*, 3537−3542.

(35) Besenbacher, F. Scanning Tunnelling Microscopy Studies of Metal Surfaces. *Rep. Prog. Phys.* **1996**, *59*, 1737−1802.

(36) Giessibl, F. J. The qPlus Sensor, a Powerful Core for the Atomic Force Microscope. *Rev. Sci. Instrum.* **2019**, *90*, 011101.

(37) Kresse, G.; Hafner, J. *Ab Initio* Molecular Dynamics for Open-Shell Transition Metals. *Phys. Rev. B* **1993**, *48*, 13115−13118.

(38) Kresse, G.; Furthmüller, J. Efficient Iterative Schemes for *Ab Initio* Total-Energy Calculations Using a Plane-Wave Basis Set. *Physical review. B, Condensed matter* **1996**, *54*, 11169−11186.

(39) Blöchl, P. E. Projector Augmented-Wave Method. *Phys. Rev. B* **1994**, *50*, 17953−17979.

(40) Kresse, G.; Joubert, D. From Ultrasoft Pseudopotentials to the Projector Augmented-Wave Method. *Phys. Rev. B* **1999**, *59*, 1758−1775.

(41) Dion, M.; Rydberg, H.; Schröder, E.; Langreth, D. C.; Lundqvist, B. I. Van der Waals Density Functional for General Geometries. *Phys. Rev. Lett.* **2004**, *92*, 246401.

(42) Hamada, I. Van der Waals Density Functional Made Accurate. *Phys. Rev. B* **2014**, *89*, 121103.

(43) Henkelman, G.; Uberuaga, B. P.; Jónsson, H. A Climbing Image Nudged Elastic Band Method for Finding Saddle Points and Minimum Energy Paths. *J. Chem. Phys.* **2000**, *113*, 9901−9904.

(44) Kästner, J.; Sherwood, P. Superlinearly Converging Dimer Method for Transition State Search. *J. Chem. Phys.* **2008**, *128*, 014106.

(45) Tersoff, J.; Hamann, D. Theory of the Scanning Tunneling Microscope. *Phys. Rev. B: Condens. Matter Mater. Phys.* **1985**, *31*, 805−813.